JOURNAL OF GEOPHYSICAL RESEARCH, VOL. 114, A09204, doi:10.1029/2009JA014126, 2009

A simulation study of particle energization observed by THEMIS spacecraft during a substorm

Maha Ashour-Abdalla,[1,2] Jean-Michel Bosqued,[3] Mostafa El-Alaoui,[1] Vahe Peroomian,[1] Meng Zhou,[1] Robert Richard,[1] Raymond Walker,[1,4] Andrei Runov,[1] and Vassilis Angelopoulos[1,4]

Received 4 February 2009; revised 28 April 2009; accepted 26 May 2009; published 9 September 2009.

[1] Energetic ions with hundreds of keV energy are frequently observed in the near-Earth tail during magnetospheric substorms. We examined the sources and acceleration of ions during a magnetospheric substorm on 1 March 2008 by using Time History of Events and Macroscale Interactions during Substorms (THEMIS) and Cluster observations and numerical simulations. Four of the THEMIS spacecraft were aligned at $y_{\mathrm{GSM}} = 6\ R_E$ during a very large substorm (AE = 1200) while the Cluster spacecraft were located about 5 R_E above the auroral ionosphere. For 2 h before the substorm, Cluster observed ionospheric oxygen flowing out into the magnetosphere. After substorm onset the THEMIS P3 and P4 spacecraft located in the near-Earth tail ($x_{\mathrm{GSM}} = -9\ R_E$ and $-8\ R_E$, respectively) observed large fluxes of energetic ions up to 500 keV. We used calculations of millions of ions of solar wind and ionospheric origin in the time-dependent electric and magnetic fields from a global magnetohydrodynamic simulation of this event to study the source of these ions and their acceleration. The simulation did a good job of reproducing the particle observations. Both solar wind protons and ionospheric oxygen were accelerated by nonadiabatic motion across large (>~5 mV/m) total electric fields (both potential and induced). The acceleration occurred in the "wall" region of the near-Earth tail where nonadiabatic motion dominates over convection and the particles move rapidly across the tail. The acceleration occurred mostly in regions with large electric fields and nonadiabatic motion. There was relatively little acceleration in regions with large electric fields and adiabatic motion or small electric fields and nonadiabatic motion. Prior to substorm onset, ionospheric ions were a significant contributor to the cross-tail current, but after onset, solar wind ions become more dominant.

Citation: Ashour-Abdalla, M., J.-M. Bosqued, M. El-Alaoui, V. Peroomian, M. Zhou, R. Richard, R. Walker, A. Runov, and V. Angelopoulos (2009), A simulation study of particle energization observed by THEMIS spacecraft during a substorm, *J. Geophys. Res.*, *114*, A09204, doi:10.1029/2009JA014126.

1. Introduction

[2] Magnetospheric substorms, the explosive releases of energy stored in the magnetotail, have been the subject of intense study for several decades [e.g., *Akasofu*, 1964; *McPherron*, 1972; *Lui*, 1996; *Baker et al.*, 1996; *Angelopoulos et al.*, 2008, and references therein]. Many aspects of substorms are still not well understood, including the effect of these events on the global circulation of ions in the magnetotail and their injection into near-Earth geosynchronous orbit.

[3] Substorm onset is characterized by dispersionless injections of energetic ions into the inner magnetosphere, during which the flux of ions of tens to hundreds of keV increase dramatically and nearly simultaneously. These injections typically occur in narrow channels, predominantly near midnight [*Belian et al.*, 1978; *Lopez et al.*, 1990; *Thomsen et al.*, 2001] and are attributed to a localized and transient increase in the electric field with a significant inductive component [e.g., *Quinn and Southwood*, 1982; *Aggson et al.*, 1983]. Observations of the plasma sheet during substorms also have highlighted the role of flows in flux transport during these periods. Studies using the AMPTE/IRM satellite indicated that the plasma sheet flows occasionally included fast but short-lived flow enhancements [*Baumjohann et al.*, 1988, 1989, 1990]. *Angelopoulos et al.* [1992] noted that these fast flows were bursty and concentrated in ~10 m intervals of enhanced flow (>400 km/s) termed bursty bulk flows (BBFs). Individual

[1]Institute of Geophysics and Planetary Physics, UCLA, Los Angeles, California, USA.
[2]Department of Physics and Astronomy, UCLA, Los Angeles, California, USA.
[3]Centre d'Etude Spatiale des Rayonnements, UPS, CNRS, Toulouse, France.
[4]Department of Earth and Space Sciences, UCLA, Los Angeles, California, USA.

0148-0227/09/2009JA014126$09.00

flow bursts frequently exceed 1000 km/s, and last for ~1 min. The occurrence of BBFs is generally correlated with *AE*, but they are found during all phases of magnetospheric activity and even during quiet times [*Angelopoulos et al.*, 1994]. More recently, *Sauvaud et al.* [1999] and *Sauvaud and Kovrazhkin* [2004] used Interball and Cluster observations to identify sporadic and recurrent injections of ions, called time-of-flight velocity dispersed ion structures (TDIS), into the inner magnetotail during substorms. The injection mechanism of TDIS was shown to operate over a wide region of the tail extending from ~7–40 R_E downtail [*Sauvaud et al.*, 1999; *Sergeev et al.*, 2000]. TDIS observations indicate that the energization and injection of ions is a sporadic process that proceeds from the outer magnetotail inward, and is related to impulsive reconnection in the midtail region [*Sergeev et al.*, 2000].

[4] The importance of ionospheric O^+ ions in the magnetotail during active times has been highlighted by a number of studies, both observational and theoretical in nature [*Sharp et al.*, 1982; *Yau et al.*, 1985; *Chappell et al.*, 1987; *Lennartsson*, 1989; *Moore and Delcourt*, 1995; *Yau and André*, 1997; *Winglee*, 1998, 2000; *Winglee et al.*, 2002; *Kistler et al.*, 2005, 2006; *Nosé et al.*, 2005, 2007; *Fok et al.*, 2006; *Moore et al.*, 2005; *Jones et al.*, 2006]. Ionospheric ions, especially oxygen, inertially load magnetospheric convection, slowing the flow speed and increasing the thermal pressure. However, the increased inertia of the flow is not the only, perhaps not even the most significant, effect which the addition of oxygen (O^+) may have on magnetospheric transport. The Larmor radius of a 10 keV oxygen ion is about 0.5 R_E in a 20 nT lobe magnetic field and a significant fraction of the plasma sheet thickness and width of the magnetotail in the much weaker magnetic field of the central plasma sheet. Thus the response of the oxygen ions to the electromagnetic fields in the plasma sheet is highly nonlocal, which may result in stresses that significantly alter the convection pattern. Moreover, heavy ions from the ionosphere might trigger substorms by decreasing the threshold for the ion tearing mode [*Baker et al.*, 1982]. Also, O^+ may enhance tail stretching during the growth phase of substorms by adding to the curvature currents [*Daglis et al.*, 1990]. On the other hand, O^+ decreases the Alfvén speed and can consequently decrease the reconnection rate, resulting in a longer expansion phase [*Shay and Swisdak.*, 2004]. Thus understanding the role of ionospheric ions is essential in understanding plasma sheet transport, acceleration and dynamics during substorms.

[5] Previous studies have investigated the role of ionospheric ions in the magnetotail by using particle tracing calculations in model electric and magnetic fields: *Cladis and Francis* [1989, 1992] investigated the centrifugal acceleration of cusp ions, *Delcourt et al.* [1989, 1993] investigated the viability of the ionospheric source, and *Peroomian and Ashour-Abdalla* [1996] calculated the quiet time densities, pressures, and other bulk parameters of the plasma sheet from the nightside auroral zone and compared the contribution of the ionosphere to that of solar wind ions from the plasma mantle. More recently, *Moore et al.* [2005] compared the non-storm-time access of ions from the ionosphere to ion access from the solar wind by using a snapshot of the fields from a global magnetohydrodynamic (MHD) simulation. Moore et al. concluded that the ionosphere and the solar wind were nearly equal contributors to the near-Earth plasma pressure during quiescent periods. *Fok et al.* [2006] used ion trajectory calculations in the electric and magnetic fields from an MHD simulation to supply the boundary condition for a substorm transport model. They found that while it takes an hour for O^+ ions to convect from the dayside to the plasma sheet they can gain 100 keV in less than a minute if they arrive when the plasma sheet dipolarization is taking place. *Winglee* [2003] used a multifluid simulation and particle calculations to argue that H^+ from the ionosphere also contributes mainly to the distant tail during steady southward IMF but that O^+ from the ionosphere can reach the near-Earth tail and be accelerated there. More recently, *Peroomian et al.* [2006] used time-dependent electric and magnetic fields from a global MHD simulation of a storm event to investigate the access of the ionosphere to the storm-time plasma sheet and ring current and compared O^+ densities and energy densities during the storm to those of solar wind ions.

[6] Particle tracing calculations also have been used to investigate the rapid energization of tail ions and dispersionless injections during substorm onset [e.g., *Delcourt and Sauvaud*, 1994; *Birn et al.*, 2000; *Zaharia et al.*, 2004]. *Delcourt and Sauvaud* [1994] used ion trajectory calculations in three-dimensional model fields of dipolarization events to show that ions were energized to high energies by the rapidly changing fields and by the transient inductive electric fields during a depolarization event. *Birn et al.* [2000] traced ion and electron trajectories in fields obtained from an MHD simulation of the magnetotail and found that energization mainly occurred in the near-Earth tail, earthward of the *x* line, and that Fermi, betatron, and nonadiabatic acceleration mechanisms were responsible for the observed energization. *Zaharia et al.* [2004] used an earthward traveling pulse superimposed on a background field to trace the gyrocenters of ions and electrons and obtained realistic particle injection signatures. *Zaharia et al.* [2004] further compared their results to previous work [*Zaharia et al.*, 2000] to show that particles energized nearer the Earth were needed to fully model the substorm injection. More recently, *Liu et al.* [2009] investigated particle injection into geosynchronous orbit by launching test particles in a model with a depolarization front. Liu et al. reproduced both the earthward injection but also the observed fast westward expansion of the injection.

[7] In this paper, we utilize a combination of global MHD simulations and particle tracing calculations, along with a state-of-the-art ionospheric O^+ outflow formulation, to address two important and interrelated questions in magnetotail physics, namely the energization and injection of ions into the inner magnetosphere, and the global dynamics of the circulation of oxygen ions in the magnetotail during a substorm event that occurred on 1 March 2008. In doing so, we place Time History of Events and Macroscale Interactions during Substorms (THEMIS) observations in the global context of magnetotail transport and acceleration. This is especially important as the THEMIS mission lacks a mass spectrometer and is largely unable to distinguish between protons and heavy ions.

[8] The paper is organized as follows. In section 2, we describe the observations by the THEMIS and Cluster spacecraft on 1 March 2008. In section 3 we describe

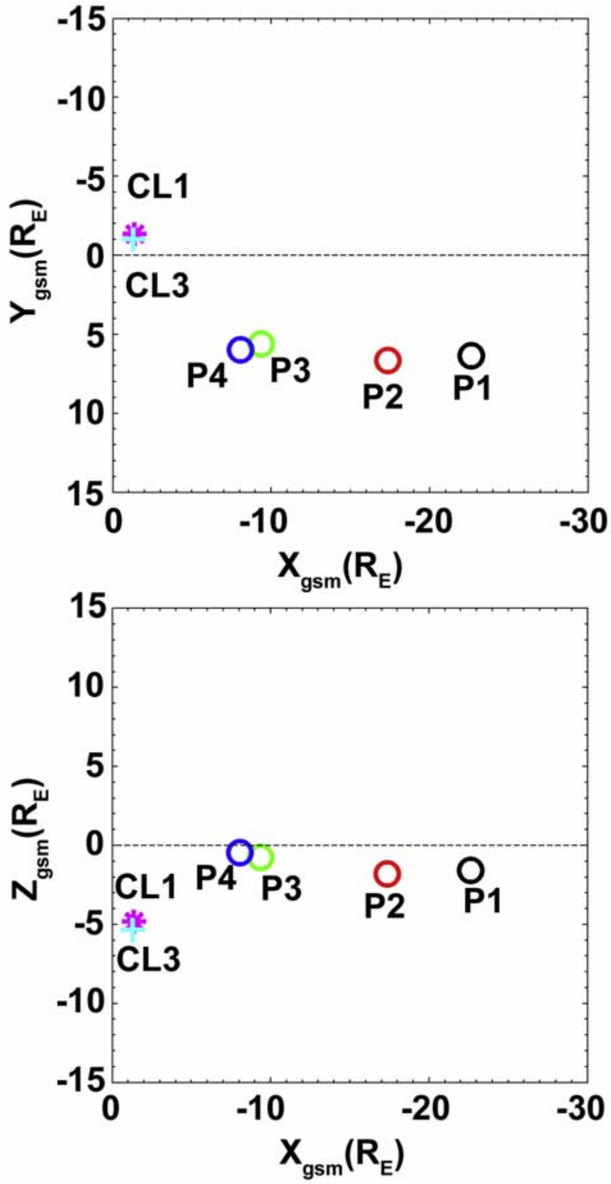

Figure 1. Positions of the Time History of Events and Macroscale Interactions during Substorms (THEMIS) and Cluster spacecraft in the (top) x_{GSM}-y_{GSM} and (bottom) x_{GSM}-z_{GSM} planes at 0155 UT on 1 March 2008.

how we studied the particle dynamics during the substorm by launching ions from the ionosphere and solar wind into the electric and magnetic fields from a global MHD simulation. The simulation results are in section 4, while in section 5 we discuss the effects of ionospheric particles and in section 6 the energization of particles is examined. Finally, in section 7 we place these results in context with previous studies and discuss the acceleration of ions during substorms.

2. Description of 1 March Observations

[9] A major magnetospheric substorm occurred at 0155 UT on 1 March 2008 when four of the THEMIS spacecraft were in conjunction. The four spacecraft were aligned approximately 6 R_E duskward of the Sun-Earth line (Figure 1). THEMIS P1 and P2 were located at $x_{GSM} = -22\ R_E$ and $x_{GSM} = -16\ R_E$ in the near-Earth tail while P3 and P4 were located closer to the Earth at $x_{GSM} = -8\ R_E$ and $-9\ R_E$, respectively. The observations during this substorm have been discussed in detail by *Runov et al.* [2008]. Auroral observations from the THEMIS all-sky camera array indicate that a pseudobreakup occurred at about 0148 UT followed by the main onset at 0155 UT. This substorm followed a period of geomagnetic activity caused by a high-speed solar wind stream, because of which the *Dst* index hovered between −25 nT and −30 nT for the previous 36 h. In addition, a large substorm (AL ∼ −800 nT) occurred at ∼2300 UT on 29 February 2008.

[10] In Figure 2 we have plotted the THEMIS P1–P4 observations during this substorm. For each spacecraft (Figures 2a–2d), the first panel shows the magnetic field, and the second and third panels contain ion energy flux spectrograms based on observations from the Solid State Telescope (SST) [*Angelopoulos*, 2008] and the Electrostatic Analyzer (ESA) [*McFadden et al.*, 2008] instruments. The fourth panel gives the density, and the fifth panel contains the velocity. The sixth and seventh panels show the energy fluxes from the energetic and thermal electrons, respectively. The dashed line at 0148 UT in Figure 2a (P1) indicates tailward flows (seventh panel) and a southward B_Z (first panel) just prior to substorm onset consistent with P1 being tailward of a neutral line. Additional tailward flows and southward B_Z were observed at 0155 UT (second dashed line).

[11] Initially the plasma sheet was hot but quiet at the location of P2 (Figure 2b). Following the pseudobreakup (left dashed line), P2 began leaving the plasma sheet since both the energetic particle flux (SST) and the thermal energy flux decreased. The spacecraft did not completely leave the plasma sheet however since the density decreased only by about a factor of two. At the same time, P2 was engulfed by fast flows moving tailward (>400 km/s). P2 then reentered the plasma sheet before leaving it again just after the main onset (second dashed line). A few minutes later it entered a region of tailward and duskward flows before entering a region of plasma sheet like particles with earthward flow. *Runov et al.* [2008] interpret this as being caused by the passage of a near-Earth neutral line tailward past P2. Starting with the pseudobreakup, P1 was always in tailward flows suggesting that it was always tailward of the neutral line. *Runov et al.* [2008] interpret these observations as evidence for substorm reconnection at about $x_{GSM} = -16\ R_E$.

[12] Perhaps the most exciting observations from this substorm were from the two earthward satellites P3 and P4. Figure 2c shows the spectrograms from P3. Prior to the pseudobreakup P3 was in the outer central plasma sheet. There was little change at the pseudobreakup but a few minutes later (0154 UT) it moved closer to the tail lobes. Following the onset at about 0158 UT there was a large increase in density coupled with increases in both the thermal and energetic electrons and protons. Note the particles of both types were accelerated to hundreds of keV (∼500 keV). The magnetic field B_X decreased consistent with motion deeper into the plasma sheet while a

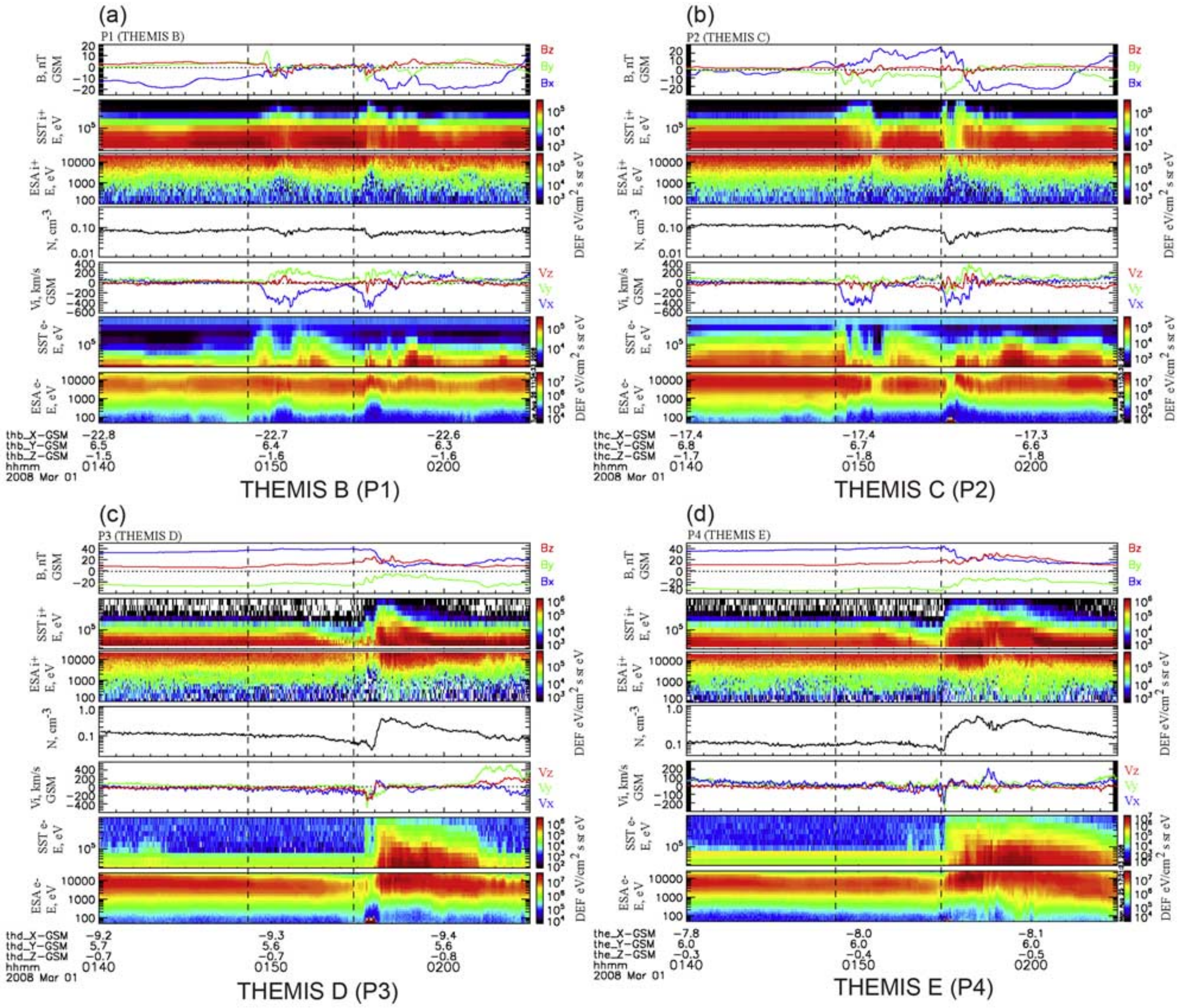

Figure 2. Observations from four of the THEMIS spacecraft on 1 March 2008. In Figures 2a–2d, the first panel shows three components of the magnetic field in GSM coordinates, the second panel contains energy flux spectrograms from the SST instrument showing energetic ions, the third panel contains energy flux spectrograms from the ESA instrument showing thermal ions, the fourth panel shows the density, the fifth panel gives the three components of the velocity in GSM coordinates, the sixth and seventh panels show electron energy flux spectrograms for the energetic and thermal particles. The dashed lines delimit the times of the pseudobreakup (0148 UT) and the main onset (0155 UT) of the substorm. Figures 2a–2d correspond to spacecraft P1, P2, P3, and P4, respectively.

significant B_Y developed. These observations are consistent with P3 being engulfed by an expanding plasma sheet. P4, closer to the Earth and the center of the plasma sheet, saw very similar changes about a minute earlier (Figure 2d).

[13] While the THEMIS spacecraft were moving through the equatorial plasma sheet, Cluster also was on the nightside. The Cluster spacecraft were at southern auroral latitudes near perigee about 5 R_E from the Earth. In Figure 3 we have plotted energy flux spectrograms from the Cluster Ion Spectrometers (CIS) on SC1 (Figure 3a) and SC3 (Figure 3b). SC1 crossed into the plasma sheet boundary layer at about 0206 UT and observed the characteristic ion energy dispersion in a velocity dispersed ion structure (VDIS) in which the highest energy particles arrive first. After several VDIS events SC1 finally entered the plasma sheet about 0219 UT. Note that the VDIS are very structured displaying beamlet like signatures. These are narrow beams of particles which characterize the VDIS [*Bosqued et al.*, 1993]. The SC3 spacecraft crossed the plasma sheet boundary about 14 min after SC1 (0220 UT). Again VDIS with beamlets were observed. At about 0222 UT SC3 moved back through the VDIS structure toward the lobes and then reentered finally reaching the central plasma sheet at about 0232 UT.

[14] One of the most significant aspects of the Cluster observations started about 2 h before the spacecraft entered the plasma sheet. In Figure 4 we have plotted the energy flux from a detector on SC3 which was observing particles coming out of the ionosphere (0–60° in pitch angle). Enhanced energy fluxes are found at very low energy

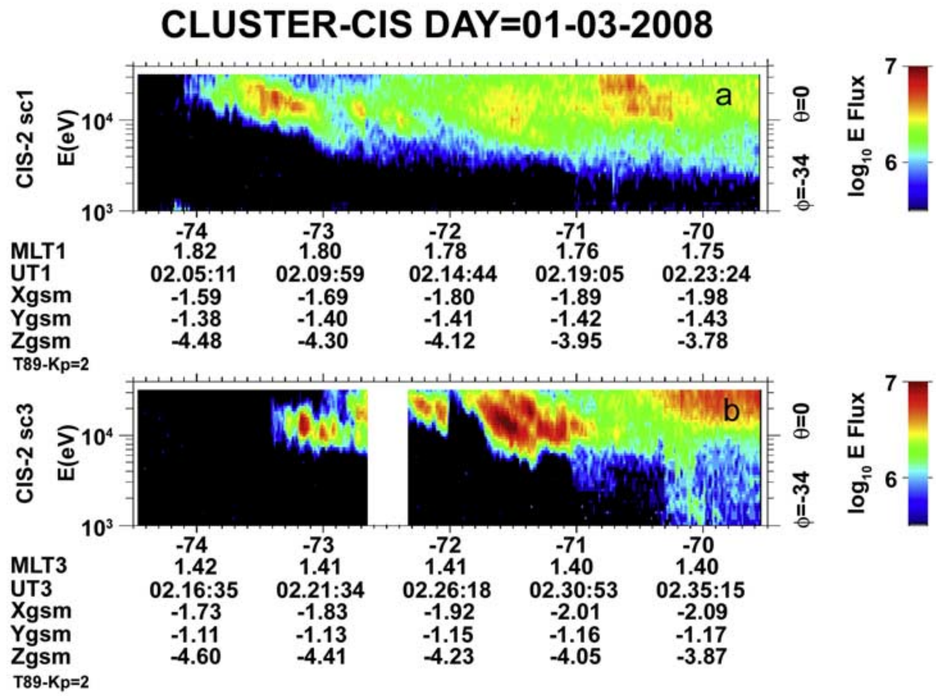

Figure 3. Cluster Ion Spectrometer (CIS) energy flux spectrogram from (a) SC1 and (b) SC3 on 1 March 2008. Figures 3a and 3b have been aligned according to latitude and are ∼11 min apart in time. VDIS were observed on SC1 starting at about 0205 UT.

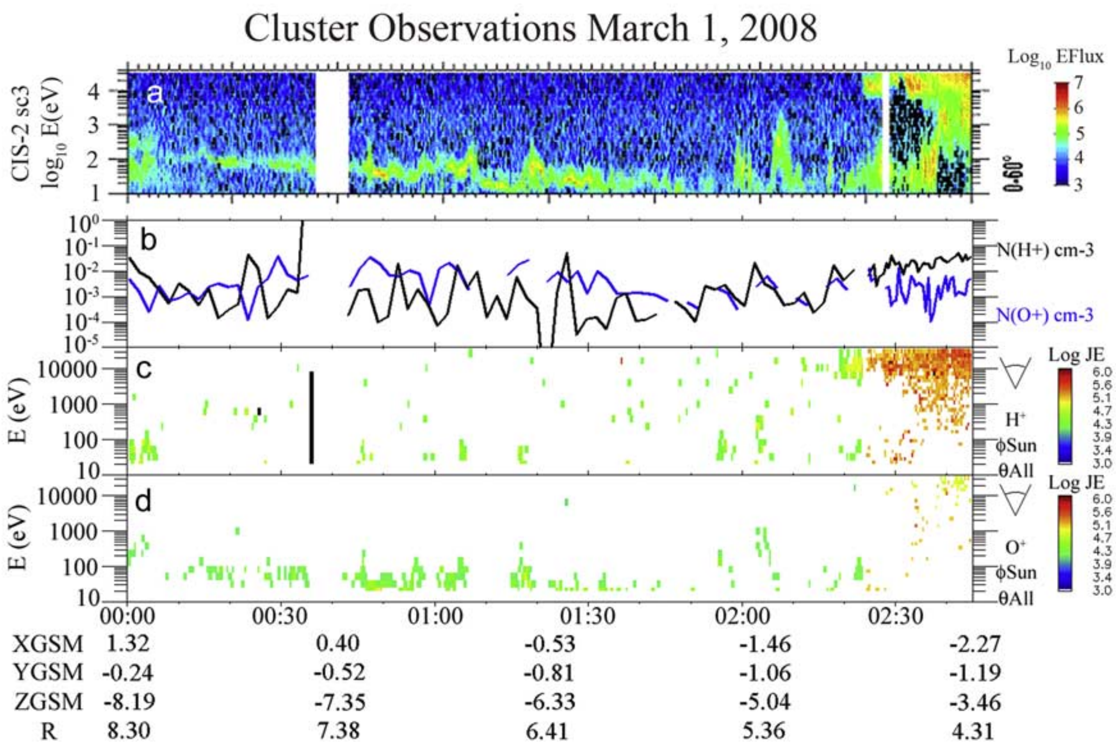

Figure 4. Cluster SC1 CIS/HIA and CODIF results for 0000–0200 UT on 1 March 2008. Plotted are (a) an energy flux spectrogram of upflowing ions, (b) the density of H^+ (black trace) and O^+ (blue trace) ions, and energy fluxes of (c) H^+, and (d) O^+ flowing away from the ionosphere.

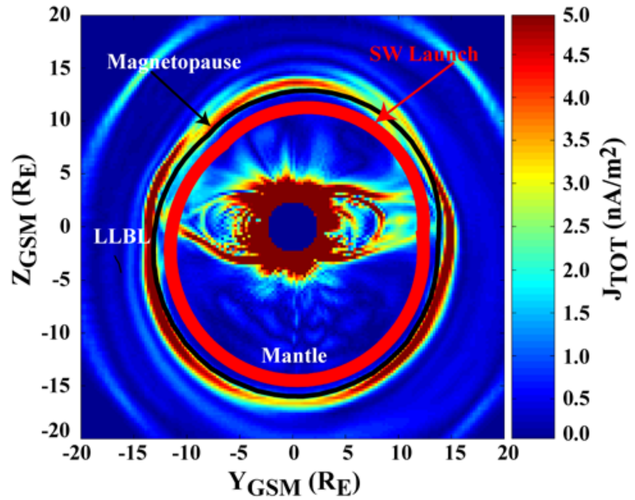

Figure 5. Cross section of the MHD total current in the x_{GSM} = 0 (terminator) plane at 0130 UT on 1 March 2008. The red annulus of thickness 1 R_E set 1 R_E inward from the inner edge of the magnetopause current layer represents the launch region for solar wind ions.

(<100 eV). Figure 4b gives the density of these particles. Throughout most of these 2 h the density is higher for O^+ (blue) than for H^+ (black). The outflow is even more dramatic in Figures 4c and 4d in which differential fluxes of the outward flowing H^+ and O^+ have been plotted. From these spectrograms it is clear that the cold particles coming from the ionosphere are O^+. The O^+ outflow in response to the geomagnetic activity and the occurrence of a prior substorm at ∼2300 UT on 29 February 2008 is consistent with observations of oxygen ion enhancements during substorms [*Mobius et al.*, 1987; *Daglis and Axford*, 1996]. Thus this event may be a very good opportunity to determine the importance of ionospheric plasma during substorms.

[15] In a companion paper, *El-Alaoui et al.* [2009] present MHD simulations of this substorm. The MHD simulation did a good job of reproducing the THEMIS observations as well as those at geosynchronous orbit. *El-Alaoui et al.* [2009] also compared their results with auroral images from the THEMIS ground all-sky camera network. They found that the simulation reproduced both the timing of the pseudobreakup and the main onset. In the simulation the substorm started with the formation of a neutral line just duskward of the THEMIS array (0142 UT). This was followed by reconnection on the dawn side of the tail (0148 UT). Later in the substorm the two x lines merged. This occurred very near substorm onset. In the more distant tail region probed by P1 and P2 a flux rope formed shortly after substorm onset. In the inner tail region probed by P3 and P4 the reconnection just duskward of THEMIS drove the tailward flow seen by P3 and P4. Finally a small vortex formed at about 0154 UT just earthward of P3 and P4. This vortex drove the duskward flows observed by these satellites.

[16] The complementary THEMIS and Cluster observations combined with the very good agreement between the MHD simulation and observations provide us with an excellent event with which to investigate both the acceleration of ions during magnetospheric substorms and the importance of ionospheric plasma during the substorm process. We have addressed these problems by using the large-scale kinetic (LSK) simulation approach in which we launch millions of particles into the time-dependent electric and magnetic fields from the MHD simulation for this event [*El-Alaoui et al.*, 2009]. For this case we included both the ionospheric and solar wind sources of ions. The calculations including the launches have been detailed in sections 3, 4, and 5.

3. Launch Schemes

[17] Observations have shown that the plasma sheet is populated by both solar wind and ionospheric plasma [e.g., *Shelley et al.*, 1972; *Sharp et al.*, 1982; *Lennartsson*, 1989; *Moore and Delcourt*, 1995]. As shown in Figure 4, Cluster observed a substantial amount of O^+ outflow as it crossed from the polar cap into the auroral zone on 1 March 2008. To model this event, one has to consider both the effect of solar wind as well as ionospheric plasma. Thus in this study we launched both H^+ solar wind and O^+ ionospheric particles. Below we describe the launch scheme for each species separately.

3.1. Solar Wind

[18] A number of previous studies have used particle tracing calculations to examine the role of the solar wind in populating the magnetosphere, each adopting a different technique for doing so. *Richard et al.* [1994, 1997] carried out test runs to determine the most viable region of solar wind entry and preferentially populated that portion of the solar wind impinging on Earth. *Peroomian et al.* [2006, 2007] launched ions at 5-min intervals on a 0.5 $R_E \times 0.5\ R_E$ grid in the y-z plane upstream of the bow shock and averaged results over 10-min time scales, and *Moore et al.* [2005] and *Fok et al.* [2006] randomly distributed ions in space and time in the solar wind. These approaches are limited by the number of ions launched per simulation [e.g., *Fok et al.*, 2006] or by the length of time results are averaged over [e.g., *Peroomian et al.*, 2007]. The investigation of the 1 March 2008 substorm required us to populate the magnetotail with statistically significant numbers of ions continuously for 2 h prior to substorm onset. In order to launch a sufficient number of ions with a reasonable computation time, we launched solar wind ions as follows: we first determined the magnetospheric cross section at x_{GSM} = 0 R_E, and identified the inner edge of the magnetopause current layer at this value of x throughout the entire interval. Then, for every 1-min interval, we randomly populated an irregular annulus of 1 R_E radial thickness adjoining the inner edge of the magnetopause current layer (Figure 5) with 500,000 ions from a T = 100 eV Maxwellian drifting tailward with 100 eV streaming energy. We launched ions beginning at 0000 UT and continued launching at 1-min intervals until 0200 UT. Using IMP-8 data, *Siscoe and Kaymaz* [1999] indicated that the plasma mantle and the plasma sheet in the flanks of the magnetosphere blend continuously into one another. *Christon et al.* [1998] used Geotail data to show that the boundary layer, composed of the plasma mantle and low-

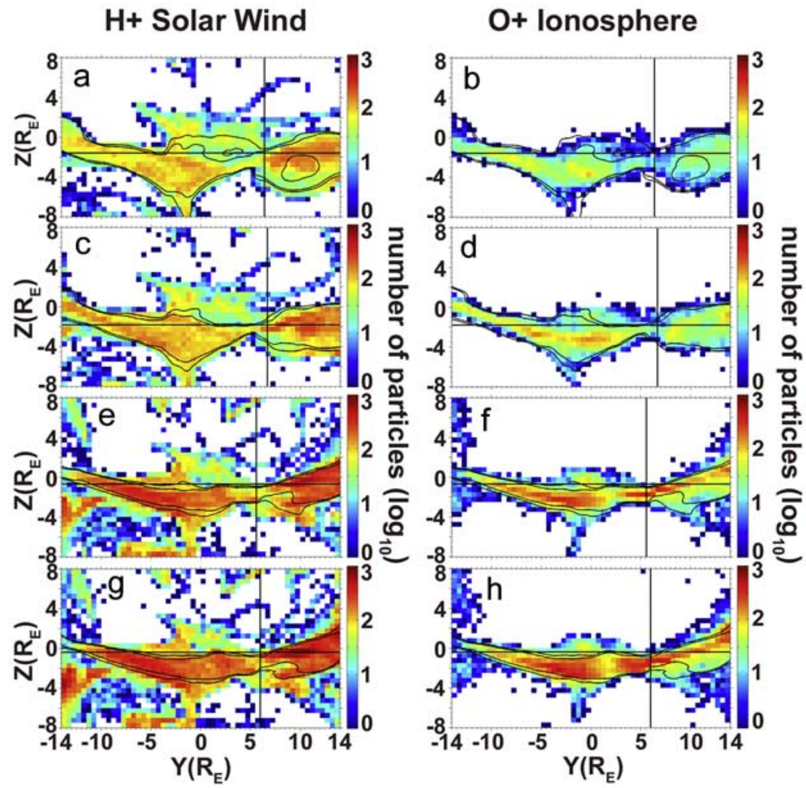

Figure 6. The y_{GSM}-z_{GSM} plots of ion counts at the *x* location of the THEMIS spacecraft at 0148 UT. (left) Solar wind H^+ ions. (right) Ionospheric O^+ ions. (a and b) Simulation results for THEMIS P1. (c–h) Same as Figures 6a and 6b for the (Figures 6c and 6d) P2, (Figures 6e and 6f) P3, and (Figures 6g and 6h) P4 spacecraft. The crosshairs show the exact location of the THEMIS spacecraft at this time.

latitude boundary layer (LLBL), was a continuous ring radially inward of the magnetopause current layer. The shell over which our launches were carried out, mimicking these observations, therefore effectively represents the contiguous plasma mantle and LLBL sources. We used the magnetosheath ion density in the MHD simulation, along with the *x* component of the MHD velocity within the launch region to normalize the flux of launched ions to the flux of solar wind ions entering the magnetosphere.

3.2. Ionosphere

[19] We launched ionospheric O^+ ions during this event by using the *Strangeway et al.* [2005] formula associating precipitating density with ion outflow. We obtained the precipitating density from the MHD simulation (with an ionospheric grid of 0.5° latitude × 3° longitude). Thus, each MHD ionospheric grid point was assigned a corresponding time-dependent outflow rate. We launched ∼250,000 O^+ ions per hemisphere per minute with a temperature of 30 eV and drift energy of 50 eV from an altitude of 1.25 R_E (r = 2.25 R_E), corresponding to the inner boundary of the MHD simulation, with the assumption that the physics of ion upflow and outflow are implicitly taken into account [e.g., *Liu et al.*, 1995; *Horwitz*, 1996; *Strangeway et al.*, 2000, 2005]. In order to avoid structuring of the outflow due to discrete sources, particles launched within each MHD ionospheric grid point were randomly distributed over the area of that grid. The outflow of O^+ ions obtained from the *Strangeway et al.* [2005] formula was nearly constant throughout this event and was ∼2.1–2.4 × 10^{26} ions/s. Ionospheric ions were launched during the same time period as solar wind ions (0000 UT to 0200 UT).

4. Simulation Results

[20] The particles in our LSK simulations are collected at a series of virtual detectors. For this study we placed plane virtual detectors in the *y-z* direction at the *x* locations of each of the THEMIS spacecraft (Figure 1). The results at the onset of the pseudobreakup (0148 UT) are plotted in Figure 6. The color spectrograms give the log of the number of particles crossing the detector with H^+ ions in Figure 6 (left) and O^+ ions in Figure 6 (right). Cross hairs give the location of the THEMIS spacecraft in the *y-z* planes. Finally we have added contours of plasma β values of 0.5 and 1.0 from the MHD simulation. In general the highest populations of particles are found within the β contours. Not surprisingly, the overall population of the plasma sheet is controlled by the magnetospheric configuration determined by the MHD simulation. Both the MHD results and the particle results exhibit complexity. The outer boundary of the plasma sheet is very irregular.

[21] Most of the particles are H^+. Both P1 and P2 are near the outer (northern) edge of the plasma sheet. At the radial distances of P1 and P2 the largest populations are just duskward of the satellites. The plasma sheet is thicker there as well. *El-Alaoui et al.* [2009] found that the tail reconnection started just duskward of midnight about 6 min

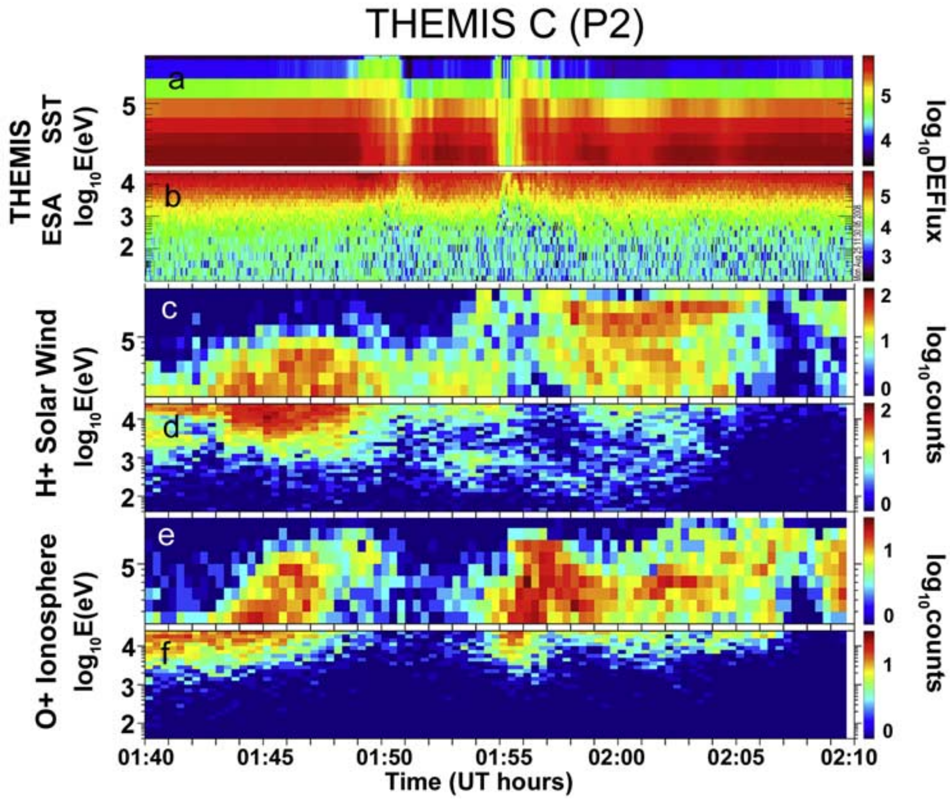

Figure 7. Comparison of observed energy flux spectrograms with counting rate spectrograms from the particle simulation for P2. Differential energy flux of (a) energetic ions from SST and (b) thermal ions from ESA. (c and d) Simulated spectrogram (in the same format) using the solar wind source particles. (e and f) Spectrograms using the ionospheric source.

earlier. The most intense particle populations are found in the P3 and P4 planes. The simulations place the spacecraft again at the northern edge of the plasma sheet and just slightly dawnward of a very large population related to the tail neutral line. Actually P3 and P4 are in a local minimum in the particle population.

[22] The O^+ population is qualitatively very similar to the H^+ population. The ionospheric oxygen has access to the entire plasma sheet. The number of particles is smaller but these count rates have not been normalized so we cannot directly compare the particle populations using this figure.

[23] In Figures 7 and 8 we present a comparison of the particle populations from our simulation with the particles observed on THEMIS. In Figure 7 we have reproduced energy versus time spectrograms from P2. The color coding in the THEMIS spectrograms gives the energy flux from the energetic ion instrument (SST) and the thermal ions (ESA) in Figures 7a and 7b. Figures 7c and 7d are energy-time spectrograms from the simulation at the SST and ESA energies. Here we have plotted the log of the counts of solar wind hydrogen ions. Similar plots for ionospheric O^+ are Figures 7e and 7f. Both the SST and ESA observations as well as the simulations indicate that THEMIS P2 was in the plasma sheet prior to 0150 UT. At about 0151 UT the observations indicate that the spacecraft briefly passed toward the lobes and then reentered the plasma sheet until about 0154 UT when it briefly exited into the lobe again. The simulated spectrogram follows the same trend as P2 observations. Specifically, at about 0150 UT the simulated energetic ion and thermal ion populations decrease much like the observations. They increase at about 0152 UT and then decreased again at 0155 UT, again much like the observations. Similar behavior is found in the O^+ populations. Both particle sources yield results that are qualitatively in agreement with the P2 observations. Examination of the MHD results [*El Alaoui et al.*, 2009] suggests that these changes are primarily due to motion of the plasma sheet with respect to P2.

[24] The most dramatic changes in the observed particles occur at the two inner spacecraft P3 and P4. In Figure 8 we have plotted both the observed and simulated spectrograms at P4. Following substorm onset at 0155 UT, P4 encountered enhanced energy fluxes of both thermal and energetic particles with energetic ions recorded up to 500 keV. The simulated H^+ counting rates exhibit similar behavior but there are some differences. For instance, both the simulated thermal and energetic ions exhibit a large decrease starting about 0150 UT. This is not evident in the observed thermal ions and only a slight decrease was observed in the energetic ions. However, the simulated particles return at the same time as the major increase in observed ions and most importantly the simulated ions show the same enhancement at energies up to 500 keV. There are virtually no ionospheric ions in the simulated population before the large increase at 0155 UT. It is interesting to note that around 0158 UT the observations show a portion of

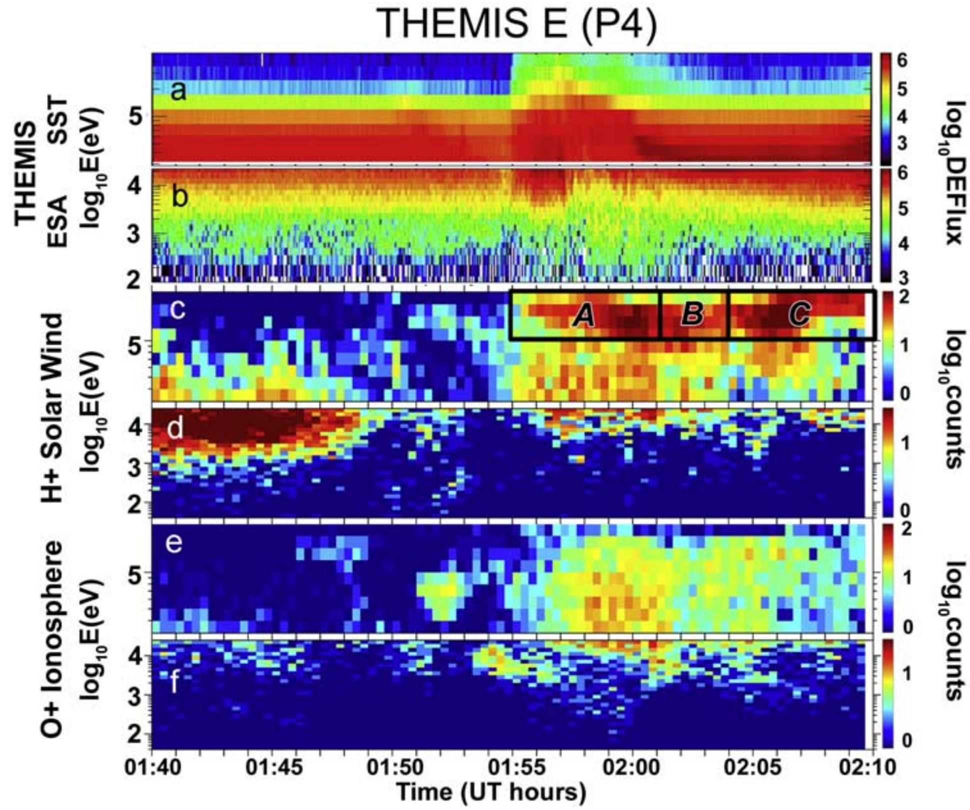

Figure 8. Comparison of observed energy flux spectrograms with counting rate spectrograms from the particle simulation for P4 in the same format as Figure 7.

detached plasma at energies of around 1 keV. This is probably is due to O^+ ions as evidenced in the simulated thermal O^+ ions in Figure 8f. The O^+ also exhibits strong fluxes at higher energies up 100 keV. Examination of the MHD model indicates that the plasma sheet boundary moved past P4 during the dropout in fluxes leaving the spacecraft near the tail lobes [*El-Alaoui et al.*, 2009]. It moved back over P4 at about 0155 UT. It appears that the plasma sheet boundary throughout this interval was nearer the spacecraft than was the actual PSBL.

[25] Spectrograms from Cluster SC1 have been plotted along with spectrograms from the simulation in Figure 9. Figures 9a–9c show the SC1 observations, and the simulated H^+ and O^+ results at the SC1 position. In Figure 9a, Cluster SC1 entered the PSBL at about 0206 UT with the largest energy fluxes starting at 0208 UT. The entry shows the characteristic dispersion of a VDIS with highest energy particles arriving at the spacecraft first. The PSBL fluxes decreased and then increased again at 0211 UT. SC1 apparently did not leave the PSBL during this decrease, since there was no inverse dispersion (low energy particles observed before the higher energy ones) during the decrease. This seems to be a temporal change. The simulated SC1 H^+ spectrogram (Figure 9b) shows similar effects with an initial entry at 0207 UT followed by a decrease and then an increase in the particles. Two more VDIS-like structures were found in the observations, starting at ~0217 UT and ~0221 UT. The VDIS-like structure starting at 0217 UT can be seen in the H^+ simulation but the one at 0221 UT is not present. In both the observations and simulation the VDIS are structured with beamlets [*Ashour-Abdalla et al.*, 2005; *Bosqued et al.*, 1993]. Note that VDIS-like structures observed later on SC1 (0217 UT and 0221 UT) have significant enhancements in O^+. In our simulations the structures starting at 0221 UT are almost entirely O^+.

5. Effect of Ionospheric Particles

[26] The comparisons in Figures 7–9 indicate that our large-scale kinetic simulation is doing a very good job of reproducing the timing of particle injections, their energy and the dispersion at five widely spaced satellites. To quantify the importance of ionospheric O^+ on the substorm dynamics we need to consider the relative density of ionospheric and solar wind particles. Recall that we did not launch ions from the solar wind, instead choosing our launch locations in the magnetopause boundary layer to save computing time. Nevertheless, the calculated densities must reflect the variations in the solar wind parameters. We do this by estimating the entry rate of the particles crossing the MHD launch area per unit time. The rate is given by $r = n_{MS} \int \mathbf{v} \cdot \mathbf{dA}$ where n_{MS} is the MHD magnetosheath density, v is the MHD velocity and the area is the particle launch area. The entry rate was estimated by using the magnetosheath density, multiplied by the MHD simulation velocity perpendicular to the launch surface. The normalization is based on a technique developed by *Ashour-Abdalla et al.* [1993]. We have modified the technique in two ways. First, we no longer assume that the streaming velocity is much larger than the thermal velocity, and second, the entry rate is

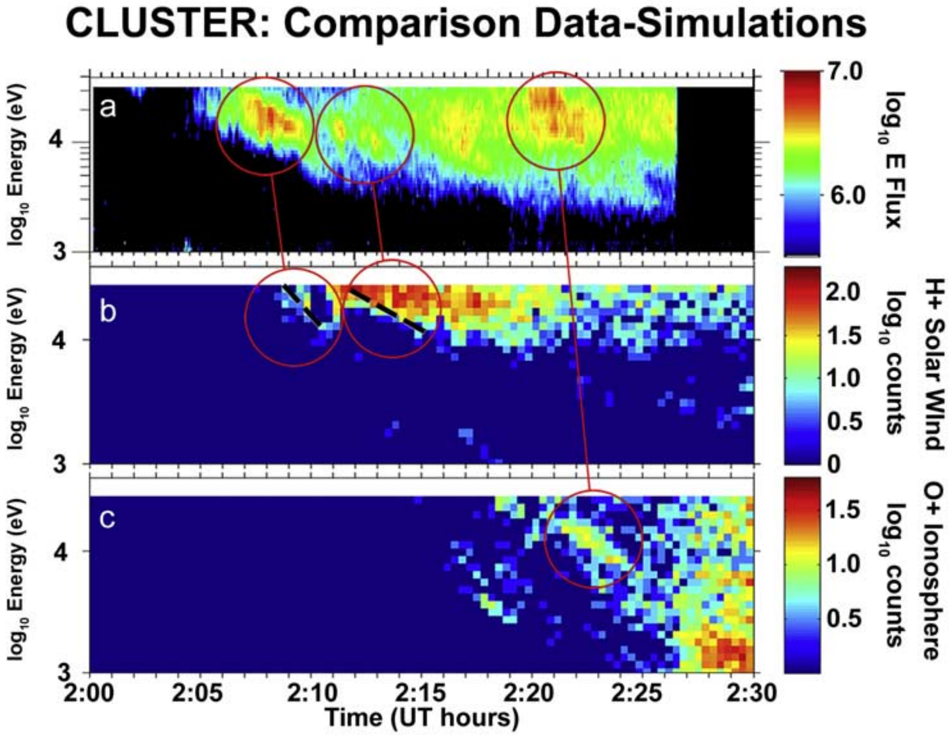

Figure 9. Comparison of Cluster observations with simulated spectrograms. (a) Cluster SC1 CIS observations of thermal ions. (b) Simulation results from the solar wind source. (c) Simulated spectrogram using particles from the ionospheric source.

not directly derived from the MHD results. The number density is given by

$$n = \sum \frac{r(t)\Delta t|v_{\perp Li}|}{NA\Delta T|v_{\perp Di}|\langle|v_{\perp Li}|\rangle} \quad (1)$$

where n is the number density, ΔT is the accumulation time at the virtual detectors, Δt is the time interval between test particle launches, N is number of test particles, $|v_{\perp Di}|$ is the absolute value of the velocity perpendicular to the detector, $|v_{\perp Li}|$ is the absolute value of the velocity perpendicular to the launch plane, $|\langle|v_{\perp Li}|\rangle$ is the average of $|v_{\perp Li}|$ over all particles in the launch, *r(t)* is the rate of particles entering the magnetosphere from the MHD model, and A is the detector area. The area and time of accumulation for particles leads to the factor $A\Delta$T in the denominator, just as in a real spacecraft detector. The rest of the equation allows us to associate the N test particles launched with the number of real particles at a given velocity. Particles moving with a lower velocity perpendicular to a plane cross that plane less often for the same density in velocity space. The factors of perpendicular velocity at the launch and detector planes correct for this. The factors related to perpendicular velocity at the launch plane did not seem to have a strong effect on the result. Other factors that come into play are the number of test particles launched N and the time interval Δt between launches. Thus, if more test particles are launched each one contributes less to the density estimate. The normalization scheme for ionospheric ions is similar to the process outlined above. However, in the case of O^+, we obtain outflow rates directly from the precipitation into the MHD ionosphere and the *Strangeway et al.* [2005] formula (see section 3.2), thus establishing a known weight for each launched particle.

[27] In Figure 10 we present a quantitative comparison between the THEMIS P3 observations and our particle simulations. The black curves give the densities of solar wind H^+ (Figure 10a) and ionospheric O^+ (Figure 10b) and the total (Figure 10c) from our simulations by using the normalization described above. The blue lines give the density determined from THEMIS P3 observations. In Figure 10a the observed density is greater than the simulation density prior to about 0154 UT while the agreement after about 0155 UT is excellent for both the slope of the change in density as well as the peak value. Prior to the pseudobreakup at 0148 UT, the O^+ density is nearly as large as the H^+ density (Figure 10b). After about 0149 UT the density of O^+ falls to less than 10% of the H^+. This shows clearly that the O^+ has its greatest effect during the first onset of the substorm and not during the main onset. Thus most of the density increase after substorm onset is solar wind H^+. In Figure 10c we have combined the O^+ density with the H^+ density, to obtain a curve that best approximates the density that would be inferred from THEMIS observations. By including both solar wind and ionospheric sources the comparison with observations improves significantly throughout the entire interval.

[28] In Figure 11 we have calculated the current density resulting from the H^+ and O^+ ions in the $y = -1\ R_E$ plane. The results at 0146 UT, just before the pseudobreakup, are plotted in Figures 11a and 11b. In the plasma sheet the H^+ current density is greater than 0.30 nA/m^2 (Figure 11a) while that from the O^+ is about half as much (Figure 11b).

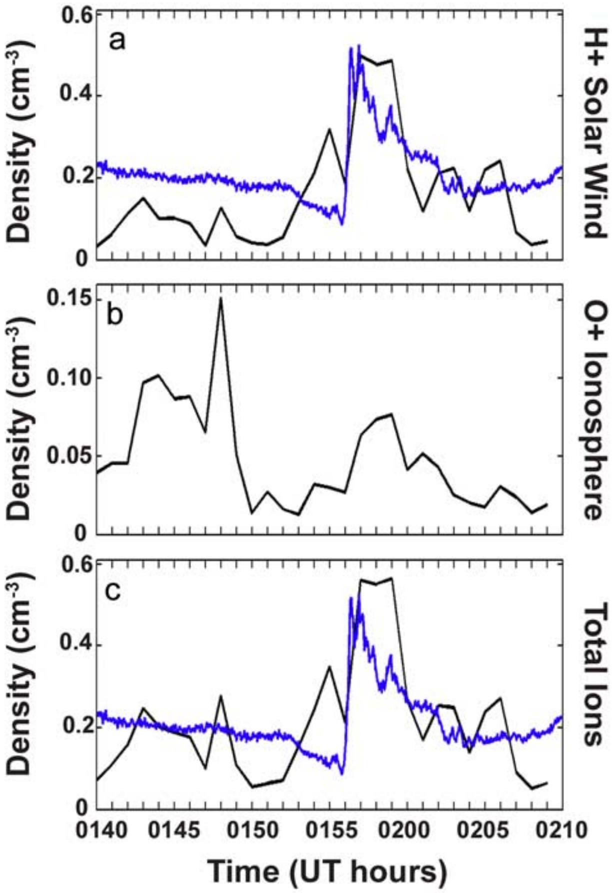

Figure 10. Comparison of ion number density observed by P3 (blue curves in Figures 10a and 10c) with simulated number density (black curves). (a) Proton density from the solar wind source. (b) O^+ density from the ionospheric source. (c) Density that P3 would observe given these two sources.

Recall that in Figure 10 this was the time interval during which the O^+ density at P3 ($-9.3\ R_E$, $5.6\ R_E$, $-0.7\ R_E$) was a substantial fraction of the H^+ density. Later at 0149 UT, following the onset of the pseudobreakup, the H^+ contribution to the current density has increased with respect to the O^+ density. Thus, during the growth phase of this substorm O^+ ions made a significant contribution to the currents in the tail and hence the overall magnetospheric configuration. Throughout the rest of the simulation H^+ ions dominated the current density. *Kistler et al.* [2005] examined three substorms, one of which was a non-storm-time substorm, by using Cluster spacecraft data in the midtail ($x_{GSM} \sim -19\ R_E$) region. Kistler et al. found that regardless of the density of O^+ ions, that species carried only 5–10% of the current density. Our results are consistent with the *Kistler et al.* [2005] observations.

6. Acceleration of Particles

[29] The most dramatic effect of this substorm is the acceleration of the energetic electrons and ions observed by the SST instrument on board THEMIS. The first step in determining the acceleration mechanism responsible for this injection is to locate the source of these ions [*Ashour-Abdalla et al.*, 2000]. In Figure 12 we have plotted the thermal pressure from the MHD simulation in the in the $x_{GSM} = 0$ launch plane (with the gray scale shown on the right) and the source locations for three sets of particles, color coded according to the number of particles. Figures 12a–12c show ions from each of three areas, identified with A, B, and C on the simulated THEMIS P4 spectrograms shown in Figure 8. Note that the "source" regions for these ions are thicker than 1 R_E. Recall the actual launch sites varied as the magnetospheric configuration changed during the substorm, thereby smearing out the source region in Figure 12. Figure 12 clearly shows that the energetic particles from all three regions came from the same launch region – the dawn side low latitude boundary layer.

[30] In order to determine the region where ions reaching the THEMIS spacecraft were accelerated and the mechanism responsible for this acceleration, we randomly chose 10 solar wind H^+ ions and 10 ionospheric O^+ ions arriving at the P3 spacecraft from each of five energy ranges ($E <$ 50 keV, 50 keV $< E <$ 100 keV, 100 keV $< E <$ 150 keV, 150 keV $< E <$ 200 keV, $E >$ 200 keV) and followed their trajectories through the electric and magnetic fields of the MHD simulation. The P3 ions were selected from those detected at the spacecraft during 0155 UT – 0156 UT. Figure 13 summarizes the results of this calculation for the P3 particles. Figures 13a–13f each give an *x-y* projection of the surface of maximum pressure, a proxy for the center of the magnetotail current sheet [*Ashour-Abdalla et al.*, 2002]. Figures 13a and 13d show the locations where ions crossed the current sheet plane, color coded according to their instantaneous energy. Figures 13b and 13e and Figures 13c and 13f show the same data color coded according to the total electric field and the inductive electric field, respectively, experienced by the ions. We estimated the inductive electric field by using the following formula: $E_{ind} = \oint \mathbf{E} \cdot dl / \oint dl$. Here E is the electric field determined at a point from the MHD simulation by interpolation, and dl is an element of a path around the given points. We choose three small square paths around the point: parallel to the *x-y*, *x-z*, and *y-z* planes. We integrated the electric field along the square paths and divide by the perimeters of the squares, giving us a vector. Finally, we computed the magnitude of this vector. The thick black curves show the location of $B_Z = 0$ at 0155 UT. Figure 13a shows that solar wind H^+ ions reaching P3 did so from a region just earthward of the x line (thick black curve) on the dawn side. Recall that the entry of particles observed at P3 (not shown) and P4 (see Figure 12) was from the dawn side LLBL. These ions gained energy rapidly and crossed the current sheet to reach the spacecraft. As will be shown below, the ions' behavior in this region is highly nonadiabatic, and the rapid acceleration and cross-tail motion of the ions is consistent with the "wall" region first reported by *Ashour-Abdalla et al.* [1992a, 1992b]. Figure 13b shows three regions of high total electric field along the solar wind ion trajectories, in the dawn flank near the x line, in the dusk flank just duskward of P3, and in a small region at $x_{GSM} \sim -12\ R_E$ and $y_{GSM} \sim -2\ R_E$. Figure 13c shows that the estimated inductive electric field also has its maximum value in the dawn region. To further illustrate the process by which solar wind ions reaching P3 are energized, we plot in Figure 14 the trajectory of an ion

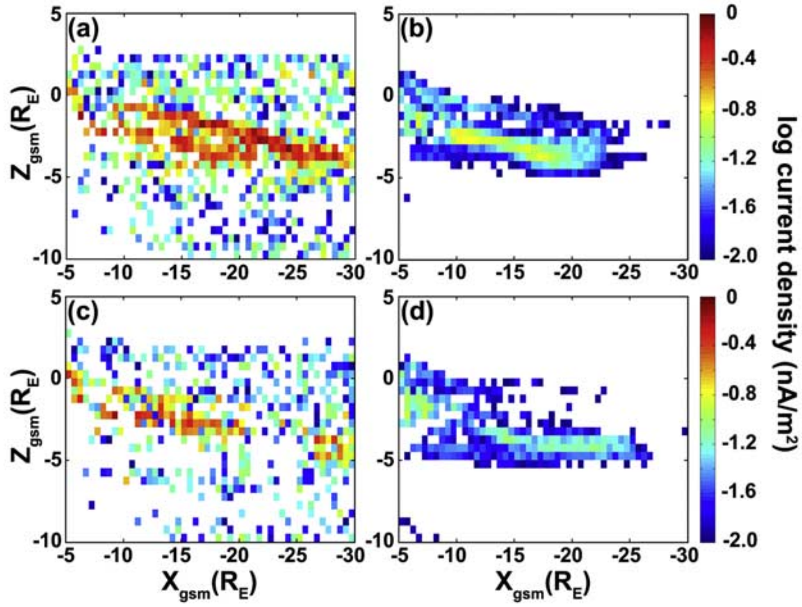

Figure 11. Simulated current density crossing the $y_{GSM} = -1\ R_E$ plane at (a and b) 0146 UT and (c and d) 0149 UT. Current densities for the (Figures 11a and 11c) solar wind source and (Figures 11b and 11e) ionospheric source are shown.

reaching the spacecraft with energy ~200 keV. Figure 14a is a 3-D rendering of the ion's orbit color coded according to its instantaneous energy. Note that the lowest energy we plot is 50 keV just to emphasize the energization. Also plotted in white are select field lines along the particle trajectory to illustrate the particle motion due to convection as well as nonadiabatic acceleration. Figures 14b–14d show the total energy (black curve) and parameter of adiabaticity κ (red curve, defined as $\sqrt{R_{c\,\min}/\rho_{L\,\max}}$, where $R_{c\min}$ is the minimum magnetic field radius of curvature and $\rho_{L\max}$ is the maximum particle Larmor radius [*Büchner and Zelenyi*, 1986, 1989]), total electric field (E_{TOT}), and a measure of the induced electric field (E_{IND}) along the particle's trajectory. The ion is launched at ~0115 UT from the dawn flank, and soon finds itself on closed field lines in that region. As the ion is carried tailward by convecting field lines, it finds itself on open field lines in the center of the tail. It then crosses onto closed field lines where it interacts with the current sheet, and gains over 150 keV in ~1 min prior to reaching P3. This also is indicated in Figure 14b, which shows that the energy gain of the ion (black curve) occurs when $\kappa \sim 1$, indicating that the ion is being accelerated nonadiabatically. The rapid increase in ion energy just prior to ~0155 UT also coincides with a region of strong inductive electric fields (Figure 14d). We note that the presence of a large E_{TOT} and E_{IND} are not sufficient to cause ion acceleration. For example, the ion shown in Figure 14 traverses a region of high E_{TOT} and E_{IND} between 0126 UT and 0140 UT, and shows no significant change in its energy (Figures 14b–14d). Rapid energization occurs only when the ion is free to move across the magnetic field, i.e., when the ion is unmagnetized and nonadiabatic.

[31] Figures 13d–13f shows the current sheet crossings of ionospheric O^+ ions that reach P3 and indicates that O^+ ions are accelerated in the same region as the solar wind H^+ ions, namely the dawnside region just earthward of the *x*

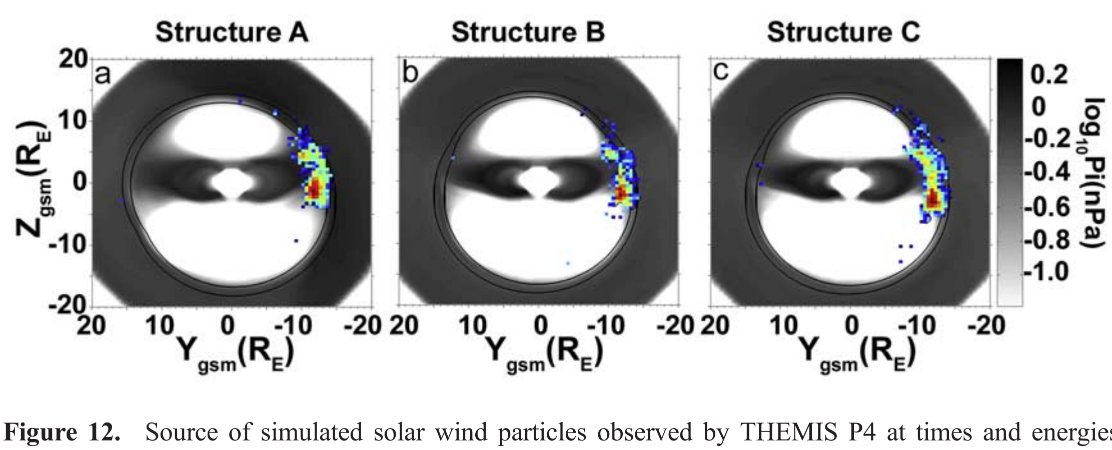

Figure 12. Source of simulated solar wind particles observed by THEMIS P4 at times and energies indicated by A, B, and C on Figure 8. The thermal pressure from the MHD simulation is shown with the gray scale on the right. The colored dots show the launch location of the ions in the source plane.

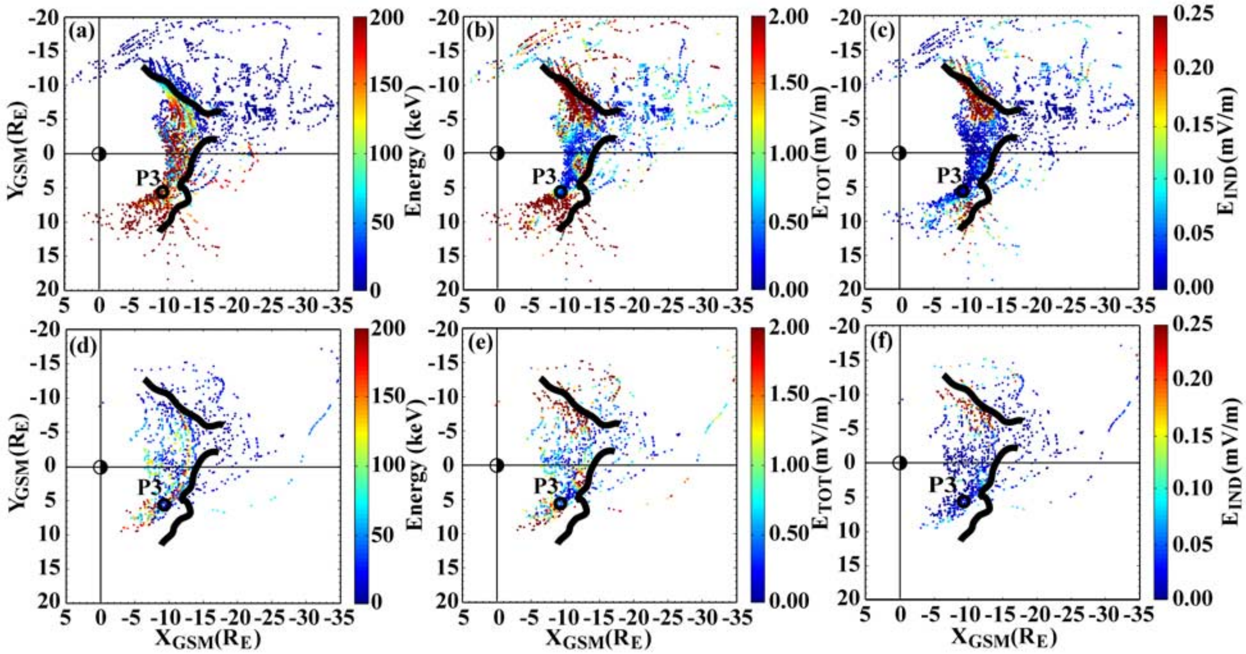

Figure 13. Crossings of the maximum pressure surface in the magnetotail by selected particles passing through a detector at P3 between 0155 UT and 0156 UT (see section 6). (a and d) Color coding give the energy of the particles. (b and e) Color coding gives the total electric field magnitude. (c and f) Color gives the induced electric field magnitude. In Figures 13a, 13b, and 13c the particles are from the solar wind source while in Figures 13d, 13e, and 13f they are the ionospheric source. The black lines show the location of the neutral lines in the tail ($B_Z = 0$) at 0155 UT.

line. Figure 15 depicts an ionospheric O^+ ion that reached P3 at ~0156 UT in the same format as Figure 14. Figure 15a shows the particle gaining energy (from blue to orange, or from ~1 keV to >100 keV) very rapidly in the dawn sector of the magnetotail as it traverses across open field lines to reach closed field lines on the dusk side. Figure 15b in fact shows that the ion gains >100 keV during a single interaction with the current sheet in a region of high E_{TOT} and E_{IND} (shown in Figures 15c and 15d). The red curve in Figure 15b shows κ as a function of time and indicates that $\kappa \ll 1$ during this interaction of the ion with the current sheet. Again, there is no energy gain associated with the high E_{TOT} and E_{IND} experienced by the oxygen ion prior to 0140 UT, when the ion is still magnetized (Figures 15c and 15d).

7. Summary and Discussion

[32] We have carried out an LSK simulation of the 1 March 2008 substorm by launching solar wind and ionospheric ions in fields obtained from a global MHD simulation of the event. We found that

[33] 1. The large-scale topology of the CPS and PSBL are determined by the MHD simulation. Ion densities and bulk parameters obtained from the LSK simulation show significant variability in space and time, in agreement with earlier results reported by *Ashour-Abdalla et al.* [2008].

[34] 2. The LSK simulation does an excellent job of reproducing THEMIS observations, including the spectrograms from the ESA and SST instruments on P2 and P4 where dropouts and intensifications match one to one with simulated spectrograms. Our simulation shows that the VDIS observed in the Cluster spectrogram is formed by H^+ ions, whereas the additional structuring in the plasma sheet is due to O^+ ions.

[35] 3. Prior to substorm onset, ionospheric O^+ ions make an appreciable contribution to the densities and current densities at the THEMIS spacecraft locations. An injection of H^+ ions at substorm onset diminishes the relative contribution of O^+. The combined density of H^+ and O^+ ions is in excellent agreement with the densities observed by THEMIS P3.

[36] 4. The strong injection of >100 keV ions observed by P3 and P4 at substorm onset results from ions originating in the dawnside LLBL and experiencing nonadiabatic acceleration in the "wall" region [*Ashour-Abdalla et al.*, 1992a, 1992b]. This region of stretched field lines is characterized by low κ, and high E_{TOT} and E_{IND}.

[37] In addition to these specific results, our MHD + LSK simulations clearly show that the mechanism of nonadiabatic acceleration, especially in the wall region, is adequate for explaining the observed ions, and no additional physics need be invoked.

[38] One of the most significant results of this study is that the simulations were able to reproduce the observed energization of ions seen by P3 and P4. In previous studies [*Ashour-Abdalla et al.*, 1992a, 1992b] using a 2-D reduction of the *Tsyganenko* [1989] magnetic field model and a uniform dawn-dusk electric field, we showed that the different regions of the plasma sheet could be characterized by varying values of κ. In the region near the *x* line, $\kappa < 1$ and the particles can be described as quasiadiabatic. In the other extreme, close to the Earth, $\kappa > 1$ and particle motion conserves the first adiabatic invariant. Between these two regions, in the wall region, $\kappa \sim 1$ and the particles are truly

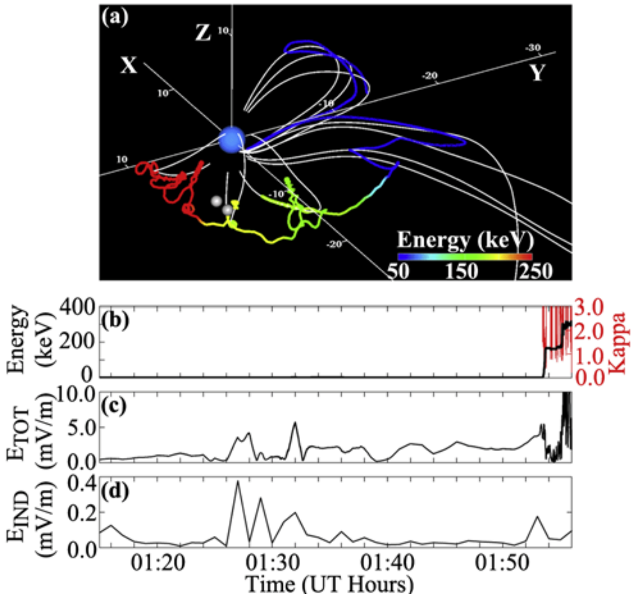

Figure 14. (a) Three-dimensional plot of the trajectory of a solar wind ion. The trajectory has been color coded with the particle's energy. The white lines are field lines along the particle's trajectory. (b) The ion energy (black curve) and the value of κ (red curve) along the trajectory as a function of time. (c) The total electric field and (d) the induced electric field as a function of time along the particle's trajectory.

chaotic. We found that particle energization was the largest in this region of the magnetotail. Examination of single particle trajectories showed that once ions entered the wall region, they moved rapidly along the y axis, gaining energy continuously while remaining trapped in the current sheet. In the present study, where we have used the three-dimensional MHD simulation to obtain electric and magnetic fields, we see similar behavior. Figures 13–15 clearly show that ions experienced rapid acceleration and duskward motion in the wall region and gain the most energy there. Figure 16 shows κ for solar wind ions crossing the current sheet plane between 1552 UT and 1553 UT. The black curves in Figure 16 show the locations of the x lines at 1555 UT. The region between the x lines stretching from $y_{GSM} \sim -10\ R_E$ to $y_{GSM} \sim 8\ R_E$, where the ion energization occurred, is clearly shown to be $1 < \kappa < 2$ (shown in red), the range of κ values delineating the wall region. However, the magnetic topology of the 3-D magnetotail is much more complicated, especially during a substorm, such that the quasiadiabatic region is mostly absent, and is instead replaced by a region populated by flux ropes tailward of $x_{GSM} \sim -15\ R_E$ resulting in high κ values (see *El-Alaoui et al.* [2009] for a complete description of the MHD simulation of this event). It is also interesting to note that the ion trajectories shown in Figures 14 and 15 clearly show that the ions never leave the current sheet in the wall region, consistent with the results found in our previous studies. When ions in the wall region encounter large electric fields directed along their motion they gain energy very rapidly (Figures 14 and 15). The appearance of the wall region in our 3-D modeling, and its profound effect on ions observed at THEMIS just after substorm onset indicates that this is a region of prime importance during substorms.

[39] Our results also highlight the importance of O^+ ions in the presubstorm period. A large substorm that occurred at 2300 UT on 29 February 2008 resulted in the outflow of O^+ ions from the ionosphere. This outflow was detected by Cluster beginning at ~0000 UT and continued for at least 2 h. Both observations [e.g., *Seki et al.*, 2001, 2002] and simulation studies [e.g., *Peroomian et al.*, 2006] have shown that outflowing O^+ can reach downtail distances from 10 R_E to tailward of 210 R_E, and that O^+ in the lobes is readily available to the magnetotail current sheet at the onset

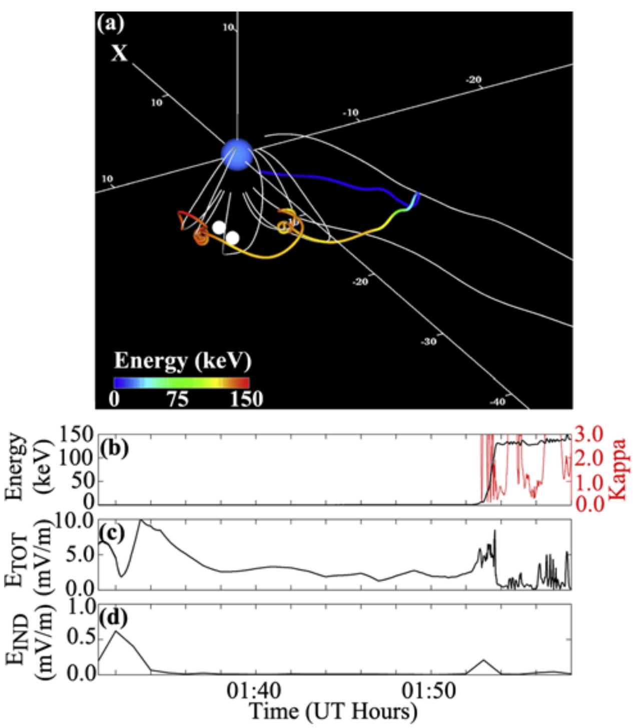

Figure 15. An ionospheric O^+ ion reaching P3 at 0155 UT–0156 UT, in the same format as Figure 14.

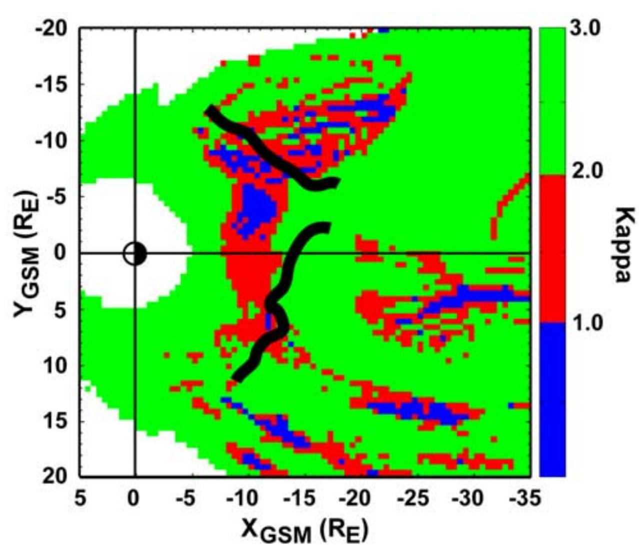

Figure 16. Average κ values for solar wind ions crossing the current sheet between 1552 UT and 1553 UT.

of activity. Whether it is in decreasing the threshold for the ion tearing mode [*Baker et al.*, 1982], enhancing tail stretching during the growth phase [*Daglis et al.*, 1990], or decreasing the Alfvén speed and consequently the reconnection rate [*Shay and Swisdak.*, 2004], O^+ ions are clearly in the right place at the right time, with significant densities. More importantly, our LSK simulation results are clearly complementary to the THEMIS observations in that the spacecraft cannot distinguish between ion species. Our results show that a significant portion of the densities measured by THEMIS, especially prior to substorm onset, is due to upflowing O^+ ions observed by the Cluster spacecraft for several hours during this event.

[40] **Acknowledgments.** The authors thank D. Schriver and J. Berchem for useful discussions. We also thank L. Kistler for help with the CODIF data and H. Kohne for help with programming and display of the data and simulation results. Research at UCLA was supported by NASA grants NNG05GG58G and NNX08AO48G. Work at CESR/CNRS was funded by Centre National d'Etudes Spatiales (CNES). The Cluster data have been kindly provided by H. Rème (CIS). We acknowledge NASA contract NAS5-02099 and V. Angelopoulos for use of data from the THEMIS Mission. Specifically, D. Larson and R. P. Lin for use of SST data, C. W. Carlson and J. P. McFadden for use of ESA data, and K. H. Glassmeier, U. Auster, and W. Baumjohann for the use of FGM data. The computing was carried out on NASA's Columbia Supercomputer. UCLA IGPP publication number 6406.

[41] Zuyin Pu thanks the reviewers for their assistance in evaluating this paper.

References

Aggson, T. L., J. P. Heppner, and N. C. Maynard (1983), Observations of large magnetospheric electric fields during the onset phase of a substorm, *J. Geophys. Res.*, *88*, 3981, doi:10.1029/JA088iA05p03981.

Akasofu, S.-I. (1964), The development of the auroral substorm, *Planet. Space Sci.*, *12*, 273, doi:10.1016/0032-0633(64)90151-5.

Angelopoulos, V. (2008), The THEMIS mission, *Space Sci. Rev.*, *141*(1–4), 5–34, doi:10.1007/s11214-008-9336-1.

Angelopoulos, V., W. Baumjohann, C. F. Kennel, F. V. Coroniti, M. G. Kivelson, R. Pellat, R. J. Walker, H. Lühr, and G. Paschmann (1992), Bursty bulk flows in the central plasma sheet, *J. Geophys. Res.*, *97*, 4027, doi:10.1029/91JA02701.

Angelopoulos, V., C. Kennel, F. Coroniti, R. Pellat, M. Kivelson, R. Walker, C. Russell, W. Baumjohann, W. Feldman, and J. Gosling (1994), Statistical characteristics of bursty bulk flow events, *J. Geophys. Res.*, *99*, 21,257, doi:10.1029/94JA01263.

Angelopoulos, V., et al. (2008), Tail reconnection triggering substorm onset, *Science*, *321*, 931, doi:10.1126/science.1160495.

Ashour-Abdalla, M., L. M. Zelenyi, J. Bosqued, V. Peroomian, Z. Wang, D. Schriver, and R. L. Richard (1992a), The formation of the wall region: Consequences in the near Earth magnetotail, *Geophys. Res. Lett.*, *19*, 1739, doi:10.1029/92GL01810.

Ashour-Abdalla, M., L. M. Zelenyi, J. M. Bosqued, V. Peroomian, Z. Wang, D. Schriver, and R. Richard (1992b), Effects of near-Earth stochastic acceleration and reflections of magnetotail ions on the formation of auroral arcs, in *Proceedings of the International Conference on Substorms (ICS-1)*, *Eur. Space Agency Spec. Publ.*, *335*, 545, Eur. Space Agency, Paris.

Ashour-Abdalla, M., J. P. Berchem, J. Büchner, and L. M. Zelenyi (1993), Shaping of the magnetotail from the mantle: Global and local structuring, *J. Geophys. Res.*, *98*, 5651, doi:10.1029/92JA01662.

Ashour-Abdalla, M., M. El-Alaoui, V. Peroomian, R. J. Walker, J. Raeder, L. A. Frank, and W. R. Paterson (2000), The origin of the near-Earth plasma population during a substorm on November 24, 1996, *J. Geophys. Res.*, *105*, 2589, doi:10.1029/1999JA900389.

Ashour-Abdalla, M., M. El-Alaoui, F. V. Coroniti, R. J. Walker, and V. Peroomian (2002), A new convection state at substorm onset: Results from an MHD study, *Geophys. Res. Lett.*, *29*(20), 1965, doi:10.1029/2002GL015787.

Ashour-Abdalla, M., J. M. Bosqued, M. El-Alaoui, V. Peroomian, L. M. Zelenyi, R. J. Walker, and J. Wright (2005), A stochastic sea: The source of plasma sheet boundary layer ion structures observed by Cluster, *J. Geophys. Res.*, *110*, A12221, doi:10.1029/2005JA011183.

Ashour-Abdalla, M., J. M. Bosqued, M. El-Alaoui, V. Peroomian, T. Umeda, and R. J. Walker (2008), Modeling PSBL high speed ion beams observed by Cluster and Double Star, *J. Adv. Space Res.*, *41*, 10, doi:10.1016/j.asr.2007.04.018.

Baker, D. N., E. W. Hones Jr., D. T. Young, and J. Birn (1982), The possible role of ionospheric oxygen in the initiation and development of plasma sheet instabilities, *Geophys. Res. Lett.*, *9*, 1337, doi:10.1029/GL009i012p01337.

Baker, D. N., T. I. Pulkkinen, V. Angelopoulos, W. Baumjohann, and R. L. McPherron (1996), Neutral line model of substorms: Past results and present view, *J. Geophys. Res.*, *101*, 12,975, doi:10.1029/95JA03753.

Baumjohann, W., G. Paschmann, N. Sckopke, C. A. Cattell, and C. W. Carlson (1988), Average ion moments in the plasma sheet boundary layer, *J. Geophys. Res.*, *93*, 11,507, doi:10.1029/JA093iA10p11507.

Baumjohann, W., G. Paschmann, and C. A. Cattell (1989), Average plasma properties in the central plasma sheet, *J. Geophys. Res.*, *94*, 6597, doi:10.1029/JA094iA06p06597.

Baumjohann, W., G. Paschmann, and H. Lühr (1990), Characteristics of high speed flow in the plasma sheet, *J. Geophys. Res.*, *95*, 3801, doi:10.1029/JA095iA04p03801.

Belian, R. D., D. N. Baker, P. R. Higbie, and E. W. Hones (1978), High-resolution energetic particle measurements at 6.6 R_E: 2. High-energy proton drift echoes, *J. Geophys. Res.*, *83*, 4857, doi:10.1029/JA083iA10p04857.

Birn, J., J. T. Gosling, M. Hesse, T. G. Forbes, and E. R. Priest (2000), Simulations of three-dimensional reconnection in the solar corona, *Astrophys. J.*, *541*, 1078, doi:10.1086/309452.

Bosqued, J. M., M. Ashour-Abdalla, M. El Alaoui, V. Peroomian, L. M. Zelenyi, and C. P. Escoubet (1993), Dispersed ion structures at the poleward edge of the auroral oval: Low-altitude observations and numerical modeling, *J. Geophys. Res.*, *98*, 19,181, doi:10.1029/93JA01143.

Büchner, J., and L. M. Zelenyi (1986), Deterministic chaos in the dynamics of charged particles near a magnetic field reversal, *Phys. Lett. A*, *118*, 395, doi:10.1016/0375-9601(86)90268-9.

Büchner, J., and L. M. Zelenyi (1989), Regular and chaotic charged particle motion in magnetotaillike field reversals: 1. Basic theory of trapped motion, *J. Geophys. Res.*, *94*, 11821, doi:10.1029/JA094iA09p11821.

Chappell, C. R., T. E. Moore, and J. H. Waite Jr. (1987), The ionosphere as a fully adequate source of plasma for the Earth's magnetosphere, *J. Geophys. Res.*, *92*, 5896, doi:10.1029/JA092iA06p05896.

Christon, S. P., et al. (1998), Magnetospheric plasma regimes identified using Geotail measurements: 2. Statistics, spatial distribution, and geomagnetic dependence, *J. Geophys. Res.*, *103*, 23,521, doi:10.1029/98JA01914.

Cladis, J. B., and W. E. Francis (1989), Transport of ions injected by AMPTE magnetotail releases, *J. Geophys. Res.*, *94*, 5497, doi:10.1029/JA094iA05p05497.

Cladis, J. B., and W. E. Francis (1992), Distribution in the magnetotail of O^+ ions from cusp/cleft ionosphere: A possible substorm trigger, *J. Geophys. Res.*, *97*, 123, doi:10.1029/91JA02376.

Daglis, I. A., and W. L. Axford (1996), Fast ionospheric response to enhanced activity in geospace: Ion feeding of the inner magnetotail, *J. Geophys. Res.*, *101*, 5047, doi:10.1029/95JA02592.

Daglis, I. A., E. T. Sarris, and G. Kremser (1990), Indications for ionospheric participation in the substorm process from AMPTE/CCE observations, *Geophys. Res. Lett.*, *17*, 57, doi:10.1029/GL017i001p00057.

Delcourt, D., and J. Sauvaud (1994), Plasma sheet ion energization during dipolarization events, *J. Geophys. Res.*, *99*, 97, doi:10.1029/93JA01895.

Delcourt, D., C. Chappell, T. Moore, and J. Waite Jr. (1989), A three-dimensional numerical model of ionospheric plasma in the magnetosphere, *J. Geophys. Res.*, *94*, 11,893, doi:10.1029/JA094iA09p11893.

Delcourt, D., J. Sauvaud, and T. Moore (1993), Polar wind ion dynamics in the magnetotail, *J. Geophys. Res.*, *98*, 9155, doi:10.1029/93JA00301.

El-Alaoui, M., M. Ashour-Abdalla, R. J. Walker, V. Peroomian, R. L. Richard, V. Angelopoulos, and A. Runov (2009), Substorm evolution as revealed by THEMIS satellites and a global MHD simulation, *J. Geophys. Res.*, doi:10.1029/2009JA014133, in press.

Fok, M.-C., T. E. Moore, P. C. Brandt, D. C. Delcourt, S. P. Slinker, and J. A. Fedder (2006), Impulsive enhancements of oxygen ions during substorms, *J. Geophys. Res.*, *111*, A10222, doi:10.1029/2006JA011839.

Horwitz, J. L. (1996), Multiscale processes in ionospheric plasma outflows, in *Physics of Space Plasmas, 1995*, edited by T. Chang and J. Jasperse, p. 227, MIT Cent. for Theor. Geo/Cosmo Plasma Phys., Cambridge, Mass.

Jones, S. T., M.-C. Fok, and P. C. Brandt (2006), Modeling global O^+ substorm injection using analytic magnetic field model, *J. Geophys. Res.*, *111*, A11S07, doi:10.1029/2006JA011607.

Kistler, L. M., et al. (2005), Contribution of nonadiabatic ions to the cross-tail current in an O^+ dominated thin current sheet, *J. Geophys. Res.*, *110*, A06213, doi:10.1029/2004JA010653.

Kistler, L. M., et al. (2006), Ion composition and pressure changes in storm time and nonstorm substorms in the vicinity of the near-Earth neutral line, *J. Geophys. Res.*, *111*, A11222, doi:10.1029/2006JA011939.

Lennartsson, W. (1989), Energetic (0.1 – to 16-keV/e) magnetospheric ion composition at different levels of solar F10.7, *J. Geophys. Res.*, *94*, 3600, doi:10.1029/JA094iA04p03600.

Liu, C., J. L. Horwitz, and P. G. Richards (1995), Effects of frictional ion heating and soft-electron precipitation on high-latitude *F* region upflows, *Geophys. Res. Lett.*, *22*, 2713, doi:10.1029/95GL02551.

Liu, W. L., X. Li, T. Sarris, C. Cully, R. Ergun, V. Angelopoulos, D. Larson, A. Keiling, K. H. Glassmeier, and H. U. Auster (2009), Observation and modeling of the injection observed by THEMIS and LANL satellites during the 23 March 2007 substorm event, *J. Geophys. Res.*, *114*, A00C18, doi:10.1029/2008JA013498.

Lopez, R., D. Sibeck, R. McEntire, and S. Krimigis (1990), The energetic ion substorm injection boundary, *J. Geophys. Res.*, *95*, 109, doi:10.1029/JA095iA01p00109.

Lui, A. (1996), Current disruption in the Earth's magnetosphere: Observations and models, *J. Geophys. Res.*, *101*, 13,067, doi:10.1029/96JA00079.

McFadden, J. P., C. W. Carlson, D. Larson, M. Ludlam, R. Abiad, B. Elliott, P. Turin, M. Marckwordt, and V. Angelopoulos (2008), The THEMIS ESA plasma instrument and in-flight calibration, *Space Sci. Rev.*, *141*, 277 – 302, doi:10.1107/s11214-008-9440-2.

McPherron, R. L. (1972), Substorm related changes in the geomagnetic tail, *Planet. Space Sci.*, *20*(9), 1521, doi:10.1016/0032-0633(72)90054-2.

Mobius, M., M. Scholer, B. Klecker, D. Hovestadt, G. Gloeckler, and F. M. Ipavich (1987), Acceleration of ions of ionospheric origin in the plasma sheet during substorm activity, in *Magnetotail Physics*, edited by A. T. Y. Lui, p. 231, Johns Hopkins Univ. Press, Baltimore, Md.

Moore, T. E., and D. C. Delcourt (1995), The geopause, *Rev. Geophys.*, *33*(2), 175, doi:10.1029/95RG00872.

Moore, T. E., et al. (2005), Plasma sheet and (nonstorm) ring current formation from solar and polar wind sources, *J. Geophys. Res.*, *110*, A02210, doi:10.1029/2004JA010563.

Nosé, M., S. Taguchi, K. Hosokawa, S. P. Christon, R. W. McEntire, T. E. Moore, and M. R. Collier (2005), Overwhelming O^+ contribution to the plasma sheet energy density during the October 2003 superstorm: Geotail/EPIC and IMAGE/LENA observations, *J. Geophys. Res.*, *110*, A09S24, doi:10.1029/2004JA010930.

Nosé, M., T. Kunori, Y. Ono, S. Taguchi, K. Hosokawa, T. E. Moore, M. R. Collier, S. P. Christon, and R. W. McEntire (2007), Simultaneous observations of ions of ionospheric origin over the ionosphere and in the plasma sheet at storm-time substorms, in *Proceedings of the Eighth International Conference on Substorms*, edited by M. Syrjäsuo and E. Donovan, p. 203, Univ. of Calgary, Alberta, Canada.

Peroomian, V., and M. Ashour-Abdalla (1996), Population of the near-Earth magnetotail from the auroral zone, *J. Geophys. Res.*, *101*, 15,387, doi:10.1029/96JA00759.

Peroomian, V., M. El-Alaoui, M. A. Abdalla, and L. M. Zelenyi (2006), Dynamics of ionospheric O^+ ions in the magnetosphere during the 24 – 25 September 1998 magnetic storm, *J. Geophys. Res.*, *111*, A12203, doi:10.1029/2006JA011790.

Peroomian, V., M. El-Alaoui, M. Ashour-Abdalla, and L. M. Zelenyi (2007), A comparison of solar wind and ionospheric plasma contributions to the September 24 – 25, 1998 magnetic storm, *J. Atmos. Sol. Terr. Phys.*, *69*, 212 – 222, doi:10.1016/j.jastp.2006.07.025.

Quinn, J., and D. Southwood (1982), Observations of parallel ion energization in the equatorial region, *J. Geophys. Res.*, *87*, 10536, doi:10.1029/JA087iA12p10536.

Richard, R. L., R. J. Walker, and M. Ashour-Abdalla (1994), The population of the magnetosphere by solar wind ions when the interplanetary magnetic field is northward, *Geophys. Res. Lett.*, *21*, 2455, doi:10.1029/94GL01427.

Richard, R. L., R. J. Walker, T. Ogino, and M. Ashour-Abdalla (1997), Flux ropes in the magnetotail: Consequences for ion populations, *Adv. Space Res.*, *20*, 1017, doi:10.1016/S0273-1177(97)00509-7.

Runov, A., V. Angelopoulos, X.-Z. Zhou, M. V. Kubyshkina, R. Nakamura, K.-H. Glassmeier, U. Auster, and H. J. Singer (2008), Multipoint in situ and ground-based observations during auroral intensifications, *J. Geophys. Res.*, *113*, A00C07, doi:10.1029/2008JA013493.

Sauvaud, J. A., and R. A. Kovrazhkin (2004), Two types of energy-dispersed ion structures at the plasma sheet boundary, *J. Geophys. Res.*, *109*, A12213, doi:10.1029/2003JA010333.

Sauvaud, J.-A., D. Popescu, D. C. Delcourt, G. K. Parks, M. Brittnacher, V. A. Sergeev, R. A. Kovrazhkin, T. Mukai, and S. Kokubun (1999), Sporadic plasma sheet ion injections into the high altitude auroral bulge-satellite observations, *J. Geophys. Res.*, *104*, 28,565, doi:10.1029/1999JA900293.

Seki, K., R. C. Elphic, M. Hirahara, T. Terasawa, and T. Mukai (2001), On atmospheric loss of oxygen ions from Earth through magnetospheric processes, *Science*, *291*, 1939, doi:10.1126/science.1058913.

Seki, K., R. C. Elphic, M. F. Thomsen, J. Bonnell, J. P. McFadden, E. J. Lund, M. Hirahara, T. Terasawa, and T. Mukai (2002), A new perspective on plasma supply mechanisms to the magnetotail from a statistical comparison of dayside mirroring O+ at low altitudes with lobe/mantle beams, *J. Geophys. Res.*, *107*(A4), 1047, doi:10.1029/2001JA900122.

Sergeev, V. A., et al. (2000), Plasma sheet ion injections into the auroral bulge: Correlative study of spacecraft and ground observations, *J. Geophys. Res.*, *105*, 18,465, doi:10.1029/1999JA900435.

Sharp, R. D., W. Lennartsson, W. K. Peterson, and E. G. Shelley (1982), The origins of the plasma in the distant plasma sheet, *J. Geophys. Res.*, *87*, 10,420, doi:10.1029/JA087iA12p10420.

Shay, M. A., and M. Swisdak (2004), Three-species collisionless reconnection: Effect of O^+ on magnetotail reconnection, *Phys. Rev. Lett.*, *93*, 175,001, doi:10.1103/PhysRevLett.93.175001.

Shelley, E. G., R. G. Johnson, and R. D. Sharp (1972), Satellite observations of energetic heavy ions during a geomagnetic storm, *J. Geophys. Res.*, *77*, 6104, doi:10.1029/JA077i031p06104.

Siscoe, G., and Z. Kaymaz (1999), Spatial relations of mantle and plasma sheet, *J. Geophys. Res.*, *104*, 14,639, doi:10.1029/1999JA900113.

Strangeway, R. J., C. T. Russell, C. W. Carlson, J. P. McFadden, R. E. Ergun, M. Temerin, D. M. Klumpar, W. K. Peterson, and T. E. Moore (2000), Cusp field-aligned currents and ion outflows, *J. Geophys. Res.*, *105*, 21,129, doi:10.1029/2000JA900032.

Strangeway, R. J., R. E. Ergun, Y.-J. Su, C. W. Carlson, and R. C. Elphic (2005), Factors controlling ionospheric outflows as observed at intermediate altitudes, *J. Geophys. Res.*, *110*, A03221, doi:10.1029/2004JA010829.

Thomsen, M. F., J. Birn, J. E. Borovsky, K. Morzinski, D. J. McComas, and G. D. Reeves (2001), Two-satellite observations of substorm injections at geo-synchronous orbit, *J. Geophys. Res.*, *106*, 8405, doi:10.1029/2000JA000080.

Tsyganenko, N. A. (1989), A magnetospheric magnetic field model with a warped tail current sheet, *Planet. Space Sci.*, *37*, 5, doi:10.1016/0032-0633(89)90066-4.

Winglee, R. M. (1998), Multi-fluid simulations of the magnetosphere: The identification of the geopause and its variation with IMF, *Geophys. Res. Lett.*, *25*, 4441, doi:10.1029/1998GL900217.

Winglee, R. M. (2000), Mapping of ionospheric outflows into the magnetosphere for varying IMF conditions, *J. Atmos. Sol. Terr. Phys.*, *62*, 527, doi:10.1016/S1364-6826(00)00015-8.

Winglee, R. M. (2003), Circulation of ionospheric and solar wind particle populations during extended southward interplanetary magnetic field, *J. Geophys. Res.*, *108*(A10), 1385, doi:10.1029/2002JA009819.

Winglee, R. M., D. Chua, M. Brittnacher, and G. K. Parks (2002), Global impact of ionospheric outflows on the dynamics of the magnetosphere and cross-polar cap potential, *J. Geophys. Res.*, *107*(A9), 1237, doi:10.1029/2001JA000214.

Yau, A. W., and M. André (1997), Sources of ion outflow in the high latitude ionosphere, *Space Sci. Rev.*, *80*, 1, doi:10.1023/A:1004947203046.

Yau, A. W., E. G. Shelley, W. K. Peterson, and L. Lenchyshyn (1985), Energetic auroral and polar ion outflow at DE 1 altitudes: Magnitude, composition, magnetic activity dependence, and long-term variations, *J. Geophys. Res.*, *90*, 8417, doi:10.1029/JA090iA09p08417.

Zaharia, S., C. Cheng, and J. Johnson (2000), Particle transport and energization associated with substorms, *J. Geophys. Res.*, *105*, 18,741, doi:10.1029/1999JA000407.

Zaharia, S., J. Birn, R. H. W. Friedel, G. D. Reeves, M. F. Thomsen, and C. Z. Cheng (2004), Substorm injection modeling with nondipolar time-dependent background field, *J. Geophys. Res.*, *109*, A10211, doi:10.1029/2004JA010464.

V. Angelopoulos, M. Ashour-Abdalla, M. El-Alaoui, V. Peroomian, R. Richard, A. Runov, R. Walker, and M. Zhou, Institute of Geophysics and Planetary Physics, UCLA, Box 951567, Los Angeles, CA 90095-1567, USA.

J.-M. Bosqued, Centre d'Etude Spatiale des Rayonnements, UPS, CNRS, BP 4346, F-31028 Toulouse, France.